An automatic algorithm for blink-artifact suppression based on iterative template matching: Application to single channel recording of cortical auditory evoked potentials

Joaquin T Valderrama[1,2,3], **Angel de la Torre**[4], **Bram Van Dun**[1,2]

[1] National Acoustic Laboratories, NSW, Australia

[2] HEARing Co-operative Research Centre, Australia

[3] Department of Linguistics, Macquarie University, NSW, Australia

[4] Department of Signal Theory, Telematics and Communications, CITIC-UGR, University of Granada, Granada, Spain

E-mail: joaquin.valderrama@nal.gov.au; joaquin.valderrama@mq.edu.au

Abstract.

Objective: Artifact reduction in electroencephalogram (EEG) signals is usually necessary to carry out data analysis appropriately. Despite the large amount of denoising techniques available with a multichannel setup, there is a lack of efficient algorithms that remove (not only detect) blink-artifacts from a single channel EEG, which is of interest in many clinical and research applications. This paper describes and evaluates the Iterative Template Matching and Suppression (ITMS), a new method proposed for detecting and suppressing the artifact associated with the blink activity from a single channel EEG.

Approach: The approach of ITMS consists of (a) an iterative process in which blink-events are detected and the blink-artifact waveform of the analyzed subject is estimated, (b) generation of a signal modeling the blink-artifact, and (c) suppression of this signal from the raw EEG. The performance of ITMS is compared with the Multi-window Summation of Derivatives within a Window (MSDW) technique using both synthesized and real EEG data.

Main results: Results suggest that ITMS presents an adequate performance in detecting and suppressing blink-artifacts from a single channel EEG. When applied to the analysis of cortical auditory evoked potentials (CAEPs), ITMS provides a significant quality improvement in the resulting responses, i.e. in a cohort of 30 adults, the mean correlation coefficient improved from 0.37 to 0.65 when the blink-artifacts were detected and suppressed by ITMS.

Significance: ITMS is an efficient solution to the problem of denoising blink-artifacts in single-channel EEG applications, both in clinical and research fields. The proposed ITMS algorithm is stable; automatic, since it does not require human intervention; low-invasive, because the EEG segments not contaminated by blink-artifacts remain unaltered; and easy to implement, as can be observed in the Matlab script implemeting the algorithm provided as supporting material.

Keywords: artifact removal, single channel EEG, quality enhancement, blinking, brain-computer interface (BCI) games

1. Introduction

The use of electroencephalogram (EEG) signals is currently very common in several research fields because of its objective and non-invasive nature [1, 2]. Some of these research fields include neuroscience [3]; evaluation of cognitive factors like attention [4], learning [5] and memory [6, 7]; linguistic development [8, 9]; and diagnosis of cognitive disorders like dyslexia [10], autism [11], and auditory processing disorder [12].

The recorded EEG signals are often contaminated by biological artifacts of different origin, such as eye-blinks, ocular movements (saccades), and muscular and cardiac activity; by non-biological factors like the amplifier noise proportional to the impedance between the electrodes and the scalp; and by electromagnetic fields induced by external sources [13]. In particular, the eye-blink artifact is among the factors that mostly degrades the quality of the EEG signals, especially in the frontal channels [14]. Therefore, the use of signal processing techniques that compensate for this undesired effect is usually necessary.

Blink-artifact removal has been approached from many different perspectives. A comprehensive review of EEG artifact removal techniques can be found in [15]. According to this review, the most used techniques reported in the literature are based on electrooculogram (EOG) subtraction, adaptive filtering, and independent component analysis (ICA).

The approach of EOG subtraction methods consists of subtracting from each analyzed EEG channel a proportion of one or more reference EOG channels containing the blink-artifacts (usually vertical and horizontal; and also radial for optimal performance) [16, 17]. The major disadvantages of these subtraction methods are that they require additional EOG channels as a reference, and that they assume there is no bidirectional contamination, i.e. that the EOGs may also be 'contaminated' by a proportion of the signal of interest, thus part of the signal of interest in the EEG would be cancelled in the subtraction process. These methods are still considered by many authors as the 'gold-standard' because of their simplicity, good performance, and low computational load [18, 19, 20].

Adaptive filtering methods consist of designing the filter parameters that minimize the error between the contaminated and the desired (free of artifact) EEG. In these methods, the filter generates a signal correlated with the artifact, which is then subtracted from the contaminated EEG [21]. These methods also require additional EOG channels as a reference to operate [22].

ICA is based on the linear mixture concept, in which the recorded EEG and EOG channels are modeled as the combination of contributions from different brain and artifact sources [23]. Artifact rejection with ICA involves a complex mathematical process consisting of (a) decomposing the EEG channels into statistically independent components, (b) selecting the components associated with the eye-blink artifact, and (c) recomposing the EEG signals without the selected artifact components [24, 25]. Although ICA can be implemented in a single-channel configuration, the optimal

performance of this technique requires the use of several EEG channels [26]. In the last decade, ICA has become very popular because of its performance [27, 28, 29], and in part, because of its easy implementation as it has been integrated into open-access signal processing toolboxes like EEGLab [30]. However, there is an ongoing debate about the quality of blink-artifact correction when decomposing and recomposing the EEG signals into independent components [18, 31, 32, 33].

The EOG subtraction, adaptive filtering, and ICA methods require a multichannel EEG configuration to operate. However, there are several clinical and research applications of EEG in which a single-channel electrode montage is used. Particularly in the audiology field, cortical auditory evoked potentials (CAEPs) recorded with a single-channel EEG setup are often used in the clinic for hearing screening and audiometric threshold estimation [34, 35], as well as in a large number of research studies, for example [36, 37, 38, 39, 40]. Additionally, there is an increasing number of brain-computer interface (BCI) applications in the fields of research and games, derived from a new generation of low-cost and portable EEG recording devices characterized by using a low number of channels and no access to EOG data [41, 42, 43].

In contrast to the large number of techniques available in multichannel applications, there has been little research in developing signal processing techniques to deal with the blink-artifact in single-channel EEG applications. The most relevant techniques to detect blink-events in single-channel EEG applications are based on amplitude-threshold, template matching, and derivatives. Amplitude-threshold based techniques consist of evaluating whether the maximum amplitude within an epoch (i.e., EEG segment containing the signal of interest and noise) exceeds a threshold, which can be set in advance by the user or automatically considering the EEG amplitude distribution [44, 45]. These methods are relatively easy to implement, but they present limitations such as (a) low accuracy, since they cannot distinguish blink-events from other high-amplitude artifacts, e.g. muscular activity or jaw movements [46]; (b) they cannot define the blink-artifact morphology or the EEG interval in which the blink-artifact occurs [47]; and (c) blink-events with the main peak component outside the limits of the epochs cannot be detected [48].

Template matching is a well-known signal processing technique for pattern recognition, which is currently being used in a variety of fields such as image processing [49, 50], signature recognition [51], stock technical analysis [52, 53], automatic classification of seismic activity [54], etc. Methods based on template matching essentially provide a distance representing the similarity between a test signal and a predefined waveform (template). A threshold must be specified for detection purposes. Template matching has been previously used in detecting blink-events in single-channel EEG applications [55, 56]. The major challenges of these methods are (a) the definition of the template, because the performance of the method would be affected if the blink-artifact morphology of a test subject does not match the template; and (b) the definition of the threshold. Both papers solve these issues by asking the user to set the threshold manually and by using a library consisting of a number of templates of

different morphology. These solutions present the inconveniences of requiring expertise from the user, which makes the method inconsistent worldwide; and dependent on the specific templates used.

A third approach for blink-artifact detection in single-channel EEG is based on the use of derivatives. These methods assume that the blink-artifacts present a triangular-shape morphology, and aim to detect abrupt changes by analyzing the derivative function of the raw EEG [57]. The multi-window summation of derivatives within a window (MSDW) technique requires the user to set a threshold manually, but it does not require a database of templates and is able to estimate the EEG intervals in which the blink-artifacts occur. MSDW presents better accuracy in detecting epochs containing blink-events compared to the amplitude-threshold and the traditional template matching approaches.

The major limitation of the aforementioned methods is that they allow detection, but not correction, of blink-artifacts. These methods have been typically used to detect and reject epochs contaminated with blink-artifacts, which eventually leads to the undesired loss of useful data [48, 16]. Unfortunately, methods able to detect and correct blink-artifacts from a single channel EEG are scarce.

The objective of this paper is to describe and evaluate a novel approach for detection and suppression of blink-artifacts in a single-channel EEG signal. The procedure is based on Iterative Template Matching and Suppression (ITMS). First, detection of blink-events is carried out by an iterative implementation of template matching, using a predefined blink-artifact template in the first iteration, and a blink-artifact waveform estimated from the test subject in the following iterations. Second, a blink-artifact signal is modeled considering the blink-artifact waveform of the subject and the positions and amplitudes of the detected blink-events. Finally, the signal modeling the blink-artifact is subtracted from the raw EEG to obtain the denoised EEG.

The performance of ITMS is evaluated with two experiments. Experiment 1 compares ITMS with the MSDW technique in terms of blink-events detection with both real and synthesized EEG data. Experiment 2 evaluates the quality improvement of real CAEP signals when blink-artifacts are detected and suppressed by the ITMS technique and by a modified version of MSDW that allows blink-artifact suppression. A software script programmed in Matlab (The Mathworks, Inc., Natick, MA) that implements the ITMS algorithm is available as supplementary material (appendix A).

2. Iterative Template Matching and Suppression (ITMS)

This section describes the mathematical formulation for the Iterative Template Matching and Suppression (ITMS) algorithm, which includes the blink-artifact estimation and its suppression from the recorded EEG.

The ITMS method assumes that the recorded EEG $y(n)$ is the summation of three uncorrelated processes: the blink-artifact $x_{blink}(n)$, the signal of interest $x_{signal}(n)$, and

noise $x_{noise}(n)$,

$$y(n) = x_{blink}(n) + x_{signal}(n) + x_{noise}(n), \tag{1}$$

where $n = 0, \ldots, N-1$, and N is the total number of samples in the EEG. The mathematical notation employed here uses parentheses to represent elements of discrete-time signals, and subindexes to represent elements of vectors. In this model, the signal of interest $x_{signal}(n)$ represents the linear and time-invariant (LTI) component of the activity of the neurons evoked by a number of stimuli. The blink-artifact $x_{blink}(n)$ is also assumed to be LTI, i.e. each blink-event produces an additive artifact with the same template, but unknown amplitude. The $x_{noise}(n)$ process includes other components, such as electromagnetic interferences, myogenic activity due to movements of the subject, spontaneous activity of the neurons, deviations from the LTI assumption in the $x_{signal}(n)$ and $x_{blink}(n)$ processes, etc.

The objective of ITMS is to obtain an estimate of the blink-artifact process $x_{blink}(n)$ in order to provide an enhanced EEG in which the blink-artifact is suppressed. According of the LTI assumption, the blink-artifact process can be modeled as the convolution of a blink-artifact template $h(n)$ ($n = 0, \ldots, L-1$) with K impulses (at positions m_k and with amplitudes A_k) representing the blink-events

$$x_{blink}(n) = h(n) * \sum_{k=1}^{K} A_k \delta(n - m_k) = \sum_{k=1}^{K} A_k \cdot h(n - m_k), \tag{2}$$

where L is the number of samples of the blink-artifact template, K is the number of blink-events, $*$ represents the convolution operator, and $\delta(n)$ is the unitary impulse at $n = 0$. As a final assumption, the amplitude of the blink-artifact is assumed to be relatively large compared to the other signals, which is consistent with the artifacts usually observed in EEG recordings.

Figure 1 shows a flowchart of the ITMS algorithm. ITMS estimates the blink-artifact (i.e. the template $h(n)$, and the parameters A_k, m_k describing the blink-events) through an iterative process, in which $h(n)$ is initialized with a predefined template $h_0(n)$. The estimation of the blink-artifact is iteratively performed by (a) detecting the blink-events through cross-correlation of the recorded EEG $y(n)$ with the template representing the blink-artifact $h(n)$, and (b) re-estimation of the blink-artifact template through averaging the EEG portions corresponding to the blink-events. This way, at each new iteration a better detection of the blink-events provides a better estimation of the blink-artifact template. After I iterations, the template $h(n)$ and the positions of the blink-events m_k are used for estimating the amplitudes of the blink-events A_k. Finally, the template and the blink-event parameters ($h(n)$, m_k and A_k) are used for estimating the blink-artifact $x_{blink}(n)$ and for suppressing it from the EEG.

This procedure provides an estimation of the blink-template specifically adapted to the subject and to the recording conditions, e.g. electrode impedances, specific location of the recording electrodes, etc. As a consequence, the blink-artifact will be optimally suppressed from the EEG. The processes involved in the proposed method are described in detail below.

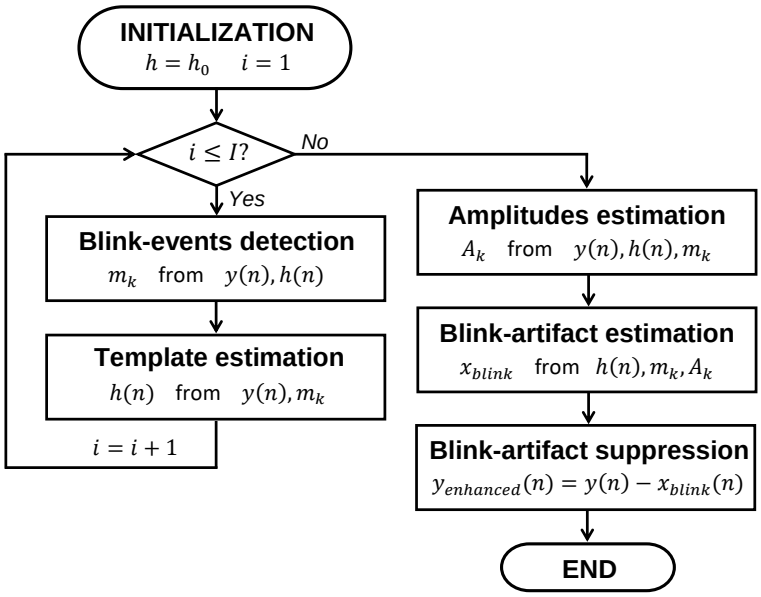

Figure 1. Iterative Template Matching and Suppression algorithm flowchart. h, blink-artifact template; h_0, predefined blink-artifact template; i, iteration; I, number of iterations; m_k, position in the EEG of detected blink-events; y, raw EEG; A_k, amplitudes of detected blink-events; x_{blink}, blink-artifact process; $y_{enhanced}$, EEG with the blink-artifact process suppressed.

2.1. Blink-events detection

At each iteration i, detection of blink-events m_k is carried out through the cross-correlation between the EEG $y(n)$ and the current blink-artifact template $h(n)$. The output of this cross-correlation function will present (a) large-amplitude peaks at the locations in the EEG with similar features as the template, i.e. the blink-artifacts, and (b) lower-amplitude peaks associated with noise and other components of the EEG. This section presents an automatic procedure to separate these two distributions.

The cross-correlation can be implemented by filtering $y(n)$ with the matched-filter, consisting in the time-reversed version of $h(n)$ [58]. Since every blink-event produces a local maximum in the matched-filter output, the local maxima of this function are candidates to be categorized as blink-events. The matched-filter output can be obtained as

$$z(n) = y(n) * h(L - 1 - n), \tag{3}$$

and it provides the cross-correlation between $y(n)$ and $h(n)$ with a delay when a causal implementation of the matched-filter is applied, i.e. there is a delay of $L - 1$ samples between each impulse generating an artifact and the corresponding local maximum in $z(n)$, since $h(L - 1 - n)$ is used instead of $h(-n)$.

Let Z_{0j} and m_{0j} be, respectively, the amplitudes and positions of the local maxima

in $z(n)$,

$$Z_{0j} = z(m_{0j}) \quad \forall\ m_{0j} \text{ verifying that } \quad z(m_{0j}) > z(m_{0j} \pm 1) \tag{4}$$

where $j = 1, \ldots, J$, and J is the total number of local maxima in $z(n)$. On one hand, the blink-events generate local maxima with large positive amplitudes in the cross-correlation function, according to the amplitude distribution of the blink-events. On the other hand, noise and other uncorrelated signals (with waveforms different to that of the template) produce a large number of random local maxima with smaller amplitudes. Therefore, the histogram of the local maxima $\{Z_{0j}\}$ is expected to show (a) a large and narrow Gaussian mode centered around zero, corresponding to the local maxima associated to noise and other uncorrelated signals; and (b) a wider mode with larger amplitudes corresponding to the blink-events.

Categorization of local maxima candidates either as blink-events or uncorrelated signals is carried out through the analysis of the histogram of local maxima. Following the approach proposed by Kim and McNames (2007) for automatic spike detection in extracellular neural recordings [59], the histogram is smoothed with a Gaussian kernel, using a 15% of the interquartile interval as bandwidth. The maximum of the smoothed histogram is associated to the mode corresponding to the uncorrelated signals, and the following minimum of the smoothed histogram on the side of positive amplitudes is used as threshold, T. The detected blink-events m_{0k} correspond to those local maxima m_{0j} with amplitude greater than the threshold, and therefore, the amplitude of the detected blink-events Z_k is

$$Z_k = z(m_{0k}) \quad \forall\ m_{0k} \text{ verifying that } \quad \begin{cases} z(m_{0k}) > z(m_{0k} \pm 1) \\ z(m_{0k}) > T \end{cases} \tag{5}$$

and the beginning of each detected blink-event is obtained as:

$$m_k = m_{0k} - L + 1 \tag{6}$$

by compensating the delay of $L - 1$ samples from the corresponding local maxima at m_{0k}, where $k = 1, \ldots, K$, and K is the number of detected blink-events. At the end of this section, the procedure for detecting the blink-events is illustrated with an example.

2.2. Estimation of the blink-artifact template

The template $h(l)$ (with $l = 0, \ldots, L - 1$) is estimated from the EEG $y(n)$ and the positions of the detected blink-events m_k. In order to estimate the template, the segments of the EEG corresponding to the detected blink-events are organized in a $K \times L$ matrix,

$$\mathbf{Y} = [y_{k,l}] \qquad y_{k,l} = y(m_k + l). \tag{7}$$

In an hypothetical situation with accurate detection (each m_k correspond to a true blink-event) the estimation would be carried out by a simple average of the EEG segments,

$$h(l) = \frac{1}{K} \sum_{k=1}^{K} y_{k,l}. \tag{8}$$

However, detection errors may occur, for example with some low-amplitude peaks corresponding to noise, or with high-amplitude peaks produced by myogenic artifacts associated with movements of the subject. These detection errors would result in inaccurate estimates of $h(l)$, and therefore, in an inaccurate detection of the blink-events in the iterative procedure. In order to prevent this problem, the template is estimated as a weighted average:

$$h_w(l) = \sum_{k=1}^{K} w_k \cdot y_{k,l} \tag{9}$$

where w_k are weights included to modulate the contribution of each sample to the average. In this work, the weights originate from a Hamming window:

$$w_k = \begin{cases} 0 & \text{if } \; r_l(k) < 0.25K \;\; \text{or} \;\; r_l(k) > 0.75K \\ 0.54 - 0.46\cos\left(4\pi \frac{r_l(k) - 0.25K}{K-1}\right) & \text{otherwise} \end{cases} \tag{10}$$

where $r_l(k)$ is the rank of $y_{k,l}$ in the set $\{y_{1,l}, y_{2,l}, \ldots, y_{K,l}\}$ (i.e. the position of $y_{k,l}$ after sorting them according to amplitude‡). This way, the estimation of the template $h(l)$ is a weighted average where all those values outside the percentiles 25-75 do not contribute, and those between these percentiles do contribute with a weight modulated by a Hamming window (the contribution of the median is maximum), and therefore the estimation of the template shares the advantages of a median-based estimation (small influence from outliers [60]) and those of a mean-based estimation (a group of samples contributes to the estimation). Because of the weighted average procedure, an accurate estimate of the blink-artifact template requires a sufficient number of detected blink-events. The weights distribution w_k is the same in all positions of the template ($l = 0, \ldots, L-1$). The mean of the resulting signal is subtracted, 20 Hz low-pass filtered (4^{th} order, Butterworth) and a linear fade-in/out of 200 ms is applied in order to remove DC level, smooth the signal and avoid discontinuities at the beginning and at the end of the template. Finally, the template is normalized,

$$h(l) = \frac{h'_w(l)}{\sqrt{\sum_{l=0}^{L-1} h'^2_w(l)}}, \tag{11}$$

where $h'_w(l)$ is the demeaned, low-pass filtered and faded-in/out version of $h_w(l)$.

The initial template $h_0(n)$ used in this study was obtained by averaging and normalizing the blink-artifact waveforms identified in a cohort of 14 normal hearing adults (8 males, 43.26 ± 7.18 yr). The detailed procedure that we followed to obtain $h_0(n)$ is provided as supplementary material (appendix B).

The performance of ITMS does not strongly depend on the initial template. Appendix C (supplementary material) presents a study of the ITMS performance when initialized with different templates: (a) the standard template described in Appendix B, (b) a single blink-artifact obtained directly from an EEG segment, (c) a synthesized biphasic rectangular pulse, (d) a monophasic rectangular pulse, (e) a triangular pulse,

‡ Because of the symmetry of the Hamming window, the weights w_k are the same when sorting in ascending or descending order.

and (f) a Hann-windowed 10 Hz tone of 1400 ms. This analysis shows that the template used to initialize ITMS is not critical, provided that the morphology of $h_0(n)$ is similar to the blink-artifact waveform typically found in the EEG. Appendix C also includes a sensitivity study of ITMS to initial templates of different lengths. This analysis shows that a duration of 1400 ms is appropriate to characterize the morphology of the blink-artifact.

2.3. Blink-artifact amplitudes

The amplitudes A_k of each blink-event are estimated from the EEG $y(n)$, the blink-artifact template $h(n)$ and the positions m_k of the detected blink-events. Taking into account the model of the EEG in equation 1, that the matched-filter consists in the casual implementation of the time-reversed version of $h(n)$ (equation 3), and that the matched-filter enhances the blink-events and attenuates the contribution of the other signals, the matched-filter output can be approximated as:

$$z(n) \approx x_{blink}(n) * h(L-1-n) = \sum_{k=1}^{K} A_k h(n-m_k) * h(L-1-n) \qquad (12)$$

From the definition and properties of the autocorrelation function $R_h(n)$ of the template,

$$R_h(n) = h(n) * h(-n) \qquad h(n-m) * h(-n) = R_h(n-m) \qquad (13)$$

the matched-filter output can be approximated as:

$$z(n) \approx \sum_{k=1}^{K} A_k R_h(n-m_k-L+1) \qquad (14)$$

Finally, if the matched-filter output is evaluated at the local maxima associated with the blink events, we obtain K equations (one for each detected blink-event):

$$Z_k = z(m_{0k}) = z(m_k+L-1) \approx \sum_{k'=1}^{K} A_{k'} R_h(m_k-m_{k'}) \qquad (15)$$

If the blink-events do not overlap (i.e. the minimum distance between successive m_k positions is greater than L), the term $R_h(m_k-m_{k'})$ is zero when $k \neq k'$, and equal to 1 when $k = k'$, since $h(n)$ is normalized. In that case, the amplitudes could be directly estimated as the value of the matched-filter output evaluated at the corresponding maximum, i.e. $A_k = Z_k$. However, when the blink-events overlap, the local maxima of the matched-filter output are affected by the overlapping events and the K equations in equation 15 should be worked out in order to estimate the amplitudes. These K equations can be written in matrix form:

$$\mathbf{Z} \approx \mathbf{R_h} \cdot \mathbf{A} \qquad (16)$$

where $\mathbf{Z}$ is a K-elements vector including the local maxima of the matched-filter output for each detected blink-event, $\mathbf{A}$ is a K-elements vector with the amplitudes of the blink-events to be estimated, and $\mathbf{R_h}$ is a $K \times K$ matrix including the autocorrelation

function evaluated at $(m_k - m_{k'})$ for each k, k' between 1 and K:

$$\mathbf{R_h} = \begin{bmatrix} R_h(m_1 - m_1) & R_h(m_1 - m_2) & \dots & R_h(m_1 - m_K) \\ R_h(m_2 - m_1) & R_h(m_2 - m_2) & \dots & R_h(m_2 - m_K) \\ \vdots & \vdots & \ddots & \vdots \\ R_h(m_K - m_1) & R_h(m_K - m_2) & \dots & R_h(m_K - m_K) \end{bmatrix} \tag{17}$$

Note that $\mathbf{R_h}$ is a quasi-diagonal symmetrical matrix, with ones in the main diagonal, values between -1 and 1 outside the diagonal, and values equal to zero for non-overlapping events (i.e. when $|m_k - m_{k'}| > L$). Since overlapping of blink-events is expected to affect only a few adjacent events, only a few diagonal blocks, in addition to the main diagonal, are expected to be non-zero. Therefore, despite the size of the $\mathbf{R_h}$ matrix, inverting it does not require a large computational load and the estimation of the amplitudes can easily be obtained as:

$$\mathbf{A} = (\mathbf{R_h})^{-1} \cdot \mathbf{Z} \tag{18}$$

2.4. Blink-artifact suppression

When both the blink template $h(n)$ and the blink-events (described by A_k and m_k) are estimated, the signal describing the blink-artifact can be estimated as:

$$x_{blink}(n) = \sum_{k=1}^{K} A_k h(n - m_k) \tag{19}$$

and the enhanced EEG can be estimated by suppressing the blink-artifact estimate:

$$y_{enhanced}(n) = y(n) - x_{blink}(n). \tag{20}$$

The performance of the ITMS method is illustrated with an example included in Figure 2. The EEG was recorded from a normal hearing adult (female, 30 yr). Figure 2.A shows a segment of an EEG, $y(n)$, in which three blink-events can be identified (blue line). The orange line represents the matched-filter output, $z(n)$. The high-amplitude local maxima in $z(n)$ ($(z(m_{0j})$, black diamonds) are candidates to be categorized as blink-events. This figure shows that the output of the matched-filter $z(n)$ presents a dominant frequency content in the low frequencies, i.e. [1-30] Hz, as a consequence of the spectral properties of the blink-artifact template. Because of the low-pass nature of the matched-filter, the number of local maxima in $z(n)$ is lower than in the EEG. This figure also shows the delay between the blink-events in the EEG and the corresponding maxima in the matched-filter output.

Figure 2.B shows the normalized histogram of the amplitudes of the local maxima (Z_{0j}), and the kernel-based smoothed histogram. This histogram shows a bimodal distribution with a large mode around zero, representing the signals not correlated with the blink template (noise and other signals); and a wider mode with larger amplitudes, representing the blink-events. The ITMS algorithm sets the threshold T that separates these two modes as the first local minimum of the smoothed histogram after the maximum corresponding to the noise mode. The local maxima candidates are categorized as blink-events if their amplitude is greater than the threshold.

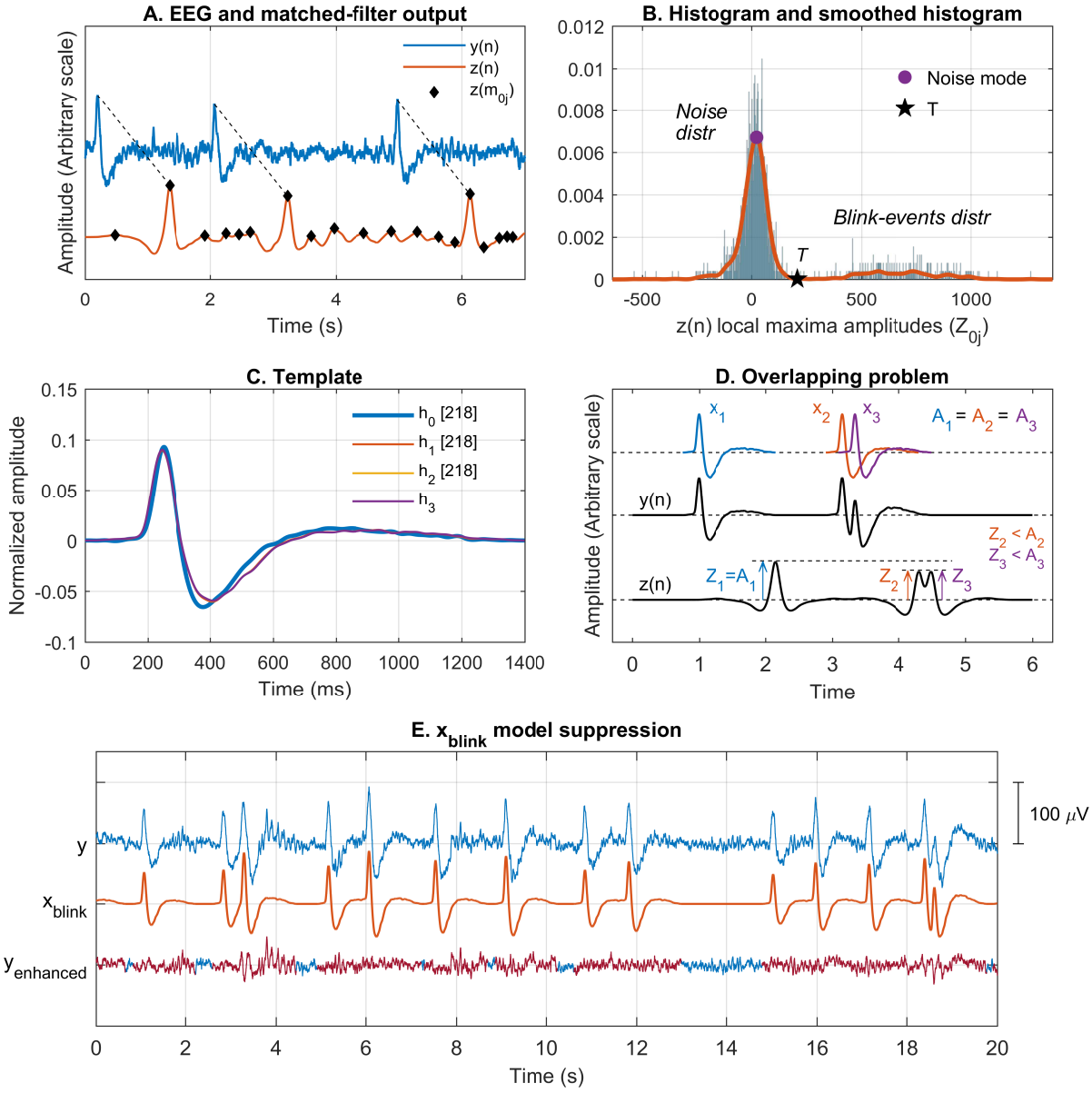

Figure 2. Details of the ITMS process. [A] Raw EEG (blue) and output of the matched-filter function $z(n)$ (orange). Local maxima of $z(n)$ ($z(m_{0j})$, black diamonds) are blink-event candidates. [B] Histogram of the local maxima amplitudes (Z_{0j}), and kernel based smoothed histogram (orange). The threshold (T) that separates the noise and the blink-events distributions is represented with a black star. [C] Initial template $h_0(n)$ and blink-artifact waveforms obtained in each iteration ($h_1(n)$ to $h_3(n)$), which are identical in this example. The total number of blink-events detected in each iteration is shown in brackets. [D] Simulation of amplitudes estimation in overlapping blink-events. [E] Suppression of the estimated blink-artifact model (x_{blink}) from the raw EEG leads to an enhanced EEG.

Figure 2.C shows the waveform morphology of the initial template $h_0(n)$ used in this study (thick blue line) and the blink-artifact templates estimated in the first three iterations ($h_1(n)$ to $h_3(n)$). This figure shows the fast convergence of the ITMS method.

Figure 2.D illustrates that the amplitudes A_k can be estimated as the value of the corresponding local maximum Z_k when the blinking-events are not overlapped, but not when they are overlapped. The top row shows three equal blink-artifact waveforms used to generate a synthesized EEG, the second signal shows the synthesized EEG $y(n)$ and the third signal is the matched-filter output $z(n)$. The first blink x_1 is not overlapped, and therefore $Z_1 = A_1$. However, due to the overlapping of the other two blinks, the amplitudes of the matched-filter output (Z_2 and Z_3) are different than those of the blinks (A_2 and A_3). In general, some degree of overlapping among blinks is expected and an accurate determination of the amplitudes requires an estimation using the proposed method.

Figure 2.E shows an example of a segment of an EEG $y(n)$ where a number of blink-events can be identified (top), the estimated blink-artifact $x_{blink}(n)$ (middle), and the enhanced EEG in which the blink-artifact has been suppressed (bottom). The modified segments in the EEG are shown in burgundy color in the $y_{enhanced}(n)$ signal. This figure shows that the portions of the EEG with no detected blink-events remain unaltered.

The experimental material presented in the assessment section, along with the example shown in figure 2, provide the verification of the initial assumptions: for a given EEG recording, the blink-artifact can be modeled as a LTI process, i.e. the blink-artifact template is stable; the amplitude of the blink-events fluctuates in a relatively wide range; and the amplitude of the blink-artifact is relatively large compared with the other signals in the EEG.

3. Assessment

The performance of the ITMS method was evaluated and compared from a dual perspective: first, we assessed the ability of ITMS to detect blink-events using real and synthesized data; and second, we evaluated using real data the effect of suppressing blink-artifacts with ITMS to improve the quality of the CAEP. This section presents the methods and results of these two experiments.

3.1. Subjects

Forty-four adults participated in this study (21 males, 44.38 ± 6.95 yr). All participants showed normal or near normal hearing sensitivity at test frequencies 0.25, 0.5, 1, 2, 3, 4, and 6 kHz. Normal hearing was considered a hearing loss $\leq$ 20 dB hearing level (HL) at 0.25–6 kHz; and near normal thresholds were defined as $\leq$ 25 dB HL up to 2 kHz, $\leq$ 30 dB HL at 3 kHz, $\leq$ 35 dB HL at 4 kHz, and $\leq$ 40 dB HL at 6 kHz [61]. Hearing thresholds were estimated in 2 dB steps with an Interacoustic AC40 audiometer (Interacoustics A/S, Middelfart, Denmark). All subjects were informed about the test

protocol, gave written consent to participate, and were paid at the end of the session to cover trip expenses. From the full set of 44 subjects tested, 14 subjects (7 males, 43.64 ± 7.30 yr) were randomly selected for estimating the predefined blink-artifact template $h_0(n)$ (details in appendix B), and the remaining 30 subjects (14 males, 44.73 ± 6.88 yr) were used in the assessment experiments.

3.2. EEG recording and analysis

The EEG recording protocol consisted of the presentation of auditory stimuli to the subjects and the recording of their associated neural response through surface gold-plated electrodes placed on the high-forehead (active), middle-forehead (ground), and right mastoid (reference). The EEG was recorded using the SmartEP auditory evoked potentials recording system and the Continuous Acquisition Module (SmartEP-CAM, Intelligent Hearing Systems, Miami, FL). The sampling frequency was 1 kHz, the gain of the preamplifier was set at 10,000, and the cut-off frequencies for the bandpass analogue filters were [1-300] Hz. The auditory stimulus consisted of a 170 ms duration /da/ synthesized in Praat [62] with a sampling frequency of 44,100 Hz. The /da/ stimulus was exported to Matlab in order to generate the stimulation sequence, which consisted of 250 repetitions of the /da/ stimulus, presented at 75 dB sound pressure level (SPL), at a fixed rate of 0.66 Hz. Thus, the duration of the sequence was about 380 seconds. The stimulation sequence was delivered monaurally on the right ear through the ER-3A insert earphones (Etymotic Research, Inc., Elk Grove Village, IL), which were connected to a Fireface UCX audio soundcard (RME Audio, Haimhausen, Germany). Stimulus level was calibrated by a type HA2 artificial ear 2-cc acoustic coupler connected to a type 4144 pressure microphone, which was connected to a type 2636 measuring amplifier through a type 2639 preamplifier cable (Brüel & Kjær Sound & Vibration Measurement A/S, Nærum, Denmark). During the EEG recording session, the subjects were lying on a comfortable couch, with their neck and shoulder muscles relaxed, while watching a movie of their choice in silent mode with subtitles. The subjects were asked to keep still during the test and to blink normally. The recording sessions took place in an electromagnetically-shielded booth at the National Acoustic Laboratories (Sydney, Australia). Analysis of recorded signals was carried out by custom scripts developed in Matlab, using the Signal Processing and the Statistics and Machine Learning Toolboxes.

This protocol is in accordance with the National Statements on Ethical Conduct in Human Research and was approved by the Macquarie University (Ref 5201400862) and by the Australian Hearing (Ref AHHREC2014-5) Human Research Ethics Committees.

3.3. Public database

One section of this study used a public database from the University of California San Diego aiming to allow any interested reader to replicate our results. This public database consists of a collection of 32-channel EEG data from 14 subjects (7 males, age not reported) recorded with a Neuroscan (Compumedics Limited, Melbourne,

Australia) recording system. Each subject folder contains 25 files of EEG data of around 200 seconds duration, recorded on two different days: 13 files recorded on the first day and 12 files recorded on the second day. The sampling frequency was 1 kHz, the bandwidth of the analog filters was [0.1-70] Hz, the reference electrode was Cz, and the ground electrode was placed on the mastoid. This public database can be downloaded from the URL: `https://sccn.ucsd.edu/~arno/fam2data/publicly_available_EEG_data.html`§.

3.4. Experiment 1. Detection of blink-events

3.4.1. Methods The performance of ITMS in detecting blink-events in synthesized EEGs was compared with MSDW [57], a technique that was specifically conceived to detect blink-events from a prefrontal EEG channel. ITMS was implemented as described in section 2 of this paper, using 10 iterations ($I = 10$). MSDW was implemented using the Matlab toolbox provided by the authors [57]. Unlike ITMS, which includes an automatic procedure to estimate the optimal threshold that separates the noise and the blink-events distributions (T), MSDW requires the user to select this threshold manually. We evaluated the performance of MSDW at the threshold suggested by the authors (threshold equal to 130) and at the threshold that we found most appropriate in the tests we did with real EEGs (threshold equal to 80).

Evaluating detection of blink-events from a single frontal EEG channel is a problem because the position of the 'true' blink-events in the EEG is not known. This handicap can be solved by two different approaches using real and synthesized data. On one hand, we artificially synthesized a number of EEGs with similar noise characteristics as real EEGs, but with the advantage that the position of the 'true' blink-events was known in advance. On the other hand, we used a public database of multichannel EEG real signals, in which the 'true' blink-events could be determined from an EEG channel positioned in the vertical of an eye, and detection performance would be evaluated from a selected EEG channel as in a single-channel EEG scenario.

The artificial EEGs were synthesized from real EEG data collected in 10 subjects (5 males, 43.70 ± 7.23 yr), selected from a subset of 30 subjects. In each subject, one EEG was synthesized consisting of noise and 300 blink-events. Each EEG was generated in three SNR conditions by modifying the level of noise with respect to the level of the blink-artifacts (signal). The evaluated SNRs were +10 dB, +5 dB, and 0 dB. The SNRs were calculated as the difference (in dB) between the root-mean-square (RMS) value of the 300 synthesized blink-artifacts and the RMS value of the noise distributions. The noise distributions of the synthesized EEGs consisted of real EEGs after removing all segments containing suspected blink-events after visual inspection. Visual inspection was repeated at least twice, and the selected EEG segments were crossfaded with a 100 ms cosine-square ramp, in order to equate the RMS value in the transition between the two segments. This procedure was followed to ensure that

§ The availability of this public database cannot be ensured by the authors of this paper.

the noise distribution of the synthesized EEGs were similar to those of real EEGs, e.g. similar spectral density, non-stationary time-series, etc. The 300 blink-events of each synthesized EEG corresponded to 30 different blink-artifact waveforms of 1.4 s duration (0.25 s pre- and 1.15 s post-local maximum) extracted from the real EEG, each of them used 10 times. The 300 blink-events were randomized, amplitude-normalized, and distributed to synthesize the artificial EEG. The distribution of the inter-blink-interval (time in milliseconds between the onsets of adjacent blink-events) was a $\sim N(2000, 600)$ distribution, i.e inter-blink-intervals followed a Normal distribution with a mean of 2000 milliseconds and a standard-deviation of 600 milliseconds. The distribution of the blink-event amplitudes A_k (in μV) followed a $\sim N(55, 14)$ distribution. These parameters approximate the real blink-event distributions observed in the 10 analyzed subjects.

The real EEGs used in this experiment corresponded to the FP1 and Fz channels of the first 10 files recorded on two different days obtained in each subject from the public database presented in section 3.3. The EEGs from the FP1 channel (positioned in the vertical of the left eye) were used to determine the 'true' blink-events, while the EEGs from the Fz channel were used to evaluate the performance of ITMS and MSDW methods in detecting blink-events. The files of day 1 in subject 'hth' were excluded from the analysis due to a calibration issue. The EEGs were digitally filtered (2^{nd} order Butterworth, [1-30] Hz). In each file, both ITMS and MSDW were applied to the EEG of the FP1 channel, and the annotation of the 'true' blink-events used as reference corresponded to events accomplishing the following three conditions: (a) the selected events were detected both by ITMS and MSDW in the FP1 channel; (b) each EEG contained at least 10 blink-events; and (c) the blink-to-EEG ratio in the FP1 channel was equal or greater than 6 dB, i.e. the energy of the blink-artifact component was at least 6 dB greater than the energy of the denoised EEG. These conditions were necessary to ensure (a) equality for both ITMS and MSDW methods, (b) a reliable estimate of h_0 in ITMS, and (c) that the blink-events categorized as 'true' had a high likelihood to be real blink-events, as was supervised and verified by visual inspection from EEG experts. An automatic annotation of the 'true' blink-events was used instead of a subjective annotation based on experts in order to provide consistency and reproducibility of this experiment. In the full dataset, a total of 167 files accomplished these conditions, and 9142 'true' blink-events were detected. ITMS was implemented as described in this paper, using 10 iterations and an initial template h_0 consisting of a single blink-artifact waveform directly extracted from an EEG in subject 'cba' (file 13, day 1). MSDW was implemented with a threshold equal to 60, since this threshold was found to be the most appropriate to detect the 'true' blink-events from the FP1 channel. The Matlab script files that allow replication of the results of this section are available as supplementary material (appendix D).

The same real and synthesized EEGs were used in the two techniques for detection purposes. Detection consisted of classifying the blink-events as: true-positive (TP), when the method correctly detected the blink-event; false-negative (FN), when the

	ITMS			$MSDW_{80}$			$MSDW_{130}$		
SNR	+10 dB	+5 dB	0 dB	+10 dB	+5 dB	0 dB	+10 dB	+5 dB	0 dB
TPR	99.47	97.50	85.00	93.27	91.47	88.90	55.07	57.40	60.87
FPPS	3.3e-4	0.0027	0.0113	9.9e-4	0.0181	0.259	1.7e-4	8.3e-4	0.0219

Table 1. True positive rate (TPR) in percentage (%) and false positives per second (FPPS) obtained at different SNRs with the ITMS method evaluated at the automatic threshold T, and with the MSDW method evaluated at the thresholds equal to 80 ($MSDW_{80}$) and equal to 130 ($MSDW_{130}$).

method did not detect a blink-event; and false-positive (FP), if the method returned a detected blink-event when that blink-event was not actually present. The TP, FN, and FP parameters were calculated for each method at different thresholds in order to generate a receiver operating characteristic (ROC) curve for each scenario. In ITMS, the thresholds varied percentage-wise in terms of the automatic threshold estimate (T): from $0.02 * T$ to T, in steps of $0.02 * T$; and from T to maximum value of Z_{0j}, in steps of $0.02 * (\max\{Z_{0j}\} - T)$. In MSDW, the thresholds varied from 2 to 200, in steps of 2. The ROC curves plot the true positive rate ($TPR = \frac{TP}{TP+FN}$) against the false positive per second ($FPPS$) rate, calculated as the ratio between the number of false positives and the total duration in seconds of the synthesized EEGs†.

3.4.2. Results Figure 3.A shows an example of a 30-seconds long EEG artificially synthesized at +10 dB SNR (top), +5 dB SNR (middle), and 0 dB SNR (bottom). Figures 3.B-D show the ROC curves for the ITMS (dark gray) and the MSDW (light gray) methods in the three analysed SNRs. These plots show that (a) both methods improve their performance as the SNR of the synthesized EEGs increases; and (b) the ITMS method presents a TPR higher than MSDW for any given FPPS in the three SNR conditions.

Table 1 shows the performance of ITMS evaluated at the automatic threshold T, and MSDW evaluated at a thresholds equal to 80 ($MSDW_{80}$) and 130 ($MSDW_{130}$), in terms of TPR and FPPS obtained at different SNRs. These results are also highlighted in figure 3 as dark-gray stars (ITMS) and light-gray stars ($MSDW_{80}$). The TPR and FPPS results for $MSDW_{130}$ are outside the limits of interest of the figure. The results shown in this table and the ROC trends in figure 3 point out that: (a) the performance of $MSDW_{130}$ is inefficient, i.e. the TPR is particularly low in the three SNR scenarios; (b) setting the threshold manually in $MSDW_{80}$ does not always result into optimal performance, as it seems to be adequate in the +5 dB SNR scenario, but it is inefficient in the other two cases (low TPR at +10 dB SNR, and high FPPS at 0 dB SNR);

† In the case of a binary detector with discrete inputs, the FPR is calculated as $FPR = \frac{FP}{FP+TN}$. However, the true-negative (TN) concept does not make sense when the input to the detector is a continuous signal, since there would be infinite true negatives. In the scenario of detection along a continuous signal, the FPR needs to be evaluated over a time interval.

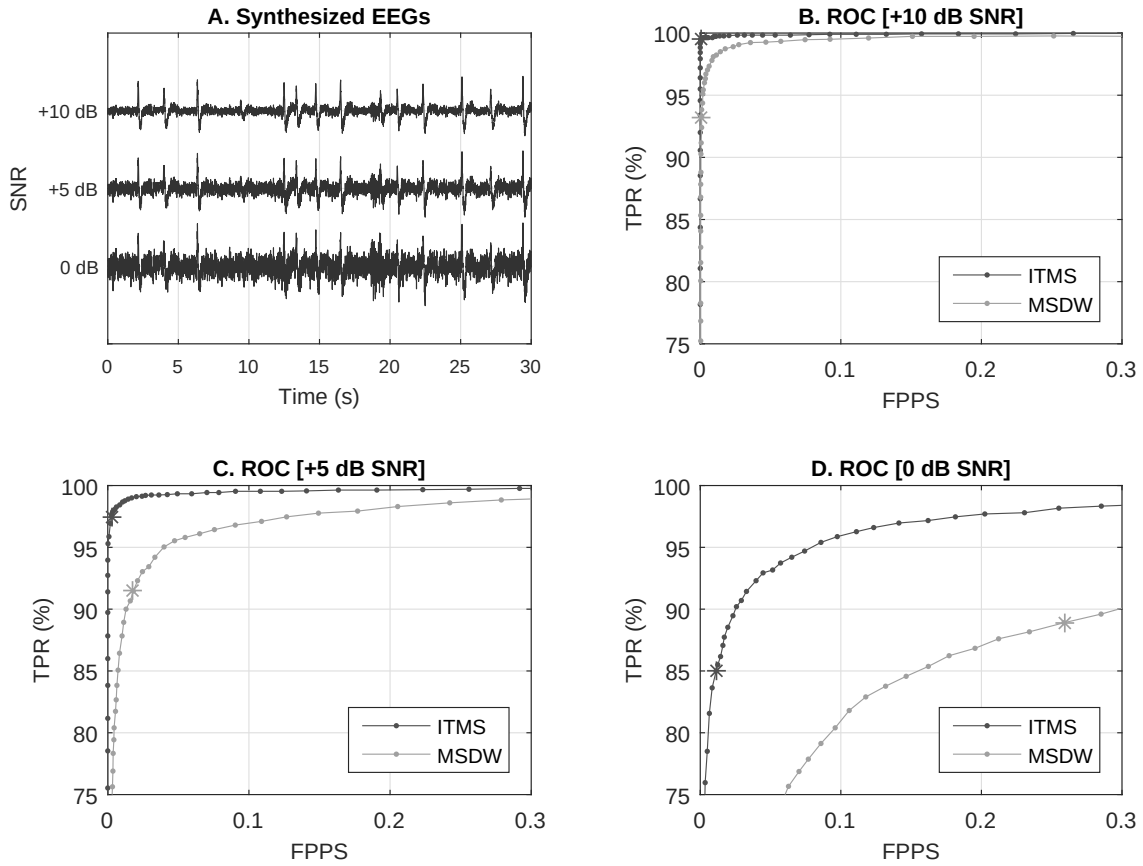

Figure 3. [A] Example of a 30-seconds long EEG synthesized at different SNRs. [B-D] ROC curves for the ITMS (dark gray) and MSDW (light gray) methods at +10 dB SNR, +5 dB SNR, and 0 dB SNR. The stars in the chart show the performance of the ITMS method at the automatic threshold (T), and the MSDW method at a threshold equal to 80 ($MSDW_{80}$). TPR: True positive rate. FPPS: False positives per second.

and (c) ITMS evaluated at the automatic threshold reaches an adequate compromise between high TPR and low FPPS in the three SNR conditions.

Figure 4 shows the ROC curve for the ITMS (dark gray) and the MSDW (light gray) methods evaluated with real data from a public database. This figure shows that (a) the performance of the ITMS method at the automatic threshold (dark-gray asterisk) presents an adequate balance of TPR and FPPS, and (b) ITMS presents a TPR higher than MSDW for any given FPPS. The mean and standard deviation of the blink-to-EEG ratios were 4.39 dB and 2.23 dB.

3.5. Experiment 2. Quality improvement of CAEPs

3.5.1. Methods The aim of this experiment was to evaluate the extent in which the ITMS and the MSDW methods improved the quality of cortical auditory evoked potentials (CAEPs) compared to the responses obtained without processing (RAW). The EEGs recorded in 30 normal hearing subjects (14 males, 44.73 ± 6.88 yr) were

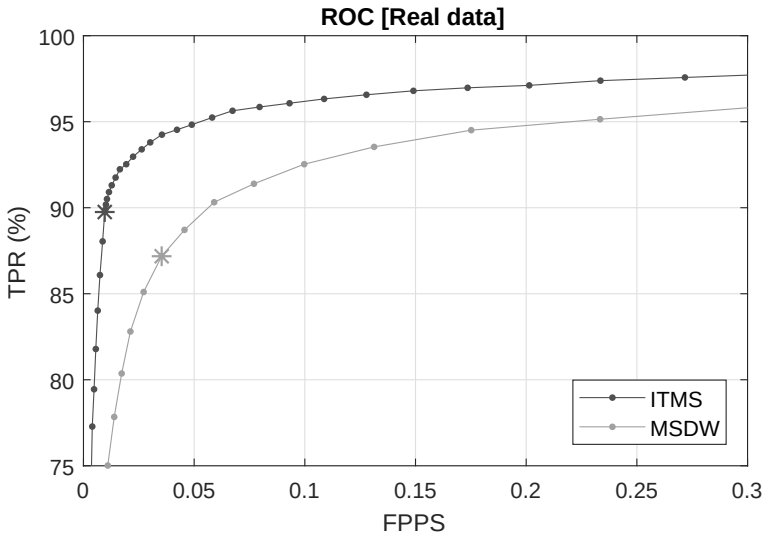

Figure 4. ROC curve for the ITMS (dark gray) and MSDW (light gray) methods evaluated with real data from a public database. TPR: True positive rate. FPPS: False positives per second. Asterisks represent the performance of ITMS at the automatic threshold T and the performance of MSDW at a threshold equal to 40.

low-pass filtered (4^{th} order Butterworth, 30 Hz), and processed with the ITMS and MSDW techniques. In MSDW, since this method does not allow correction of the blink-artifact (only detection), we obtained the processed EEGs by linear interpolation of the detected blink-events boundaries. We implemented MSDW at the threshold in which best performance was observed (threshold equal to 80). The EEGs processed with ITMS corresponded to the $y_{enhanced}(n)$ signals, described in section 2, in which the blink-artifacts were suppressed.

As presented in section 3.2, the recorded EEGs contained the neural responses evoked by 250 /da/ stimuli. In each EEG, we obtained five different CAEP signals by averaging and demeaning five blocks of 50 sweeps (EEG segments corresponding to the first 300 ms from the stimulus onset). The quality of the signals was estimated in terms of their reproducibility by calculating the correlation coefficient (r) between all possible combinations of the five CAEPs, taken two at a time (10 statistics per subject) [63]. Thus, we obtained an r-distribution of 300 statistics (30 subjects) for the RAW, MSDW, and ITMS scenarios.

Since none of the three r-distributions were normally distributed (p-values were statistically significant in the Lilliefors normality test), the three r-distributions were compared by the non-parametric Kruskal-Wallis analysis of variance test, applying the Tukey-Kramer correction for multiple comparisons. Statistic significance was achieved for p-values lower than 0.05 [64].

3.5.2. Results Figure 5.A shows an example of an unprocessed EEG segment (RAW), and processed with the MSDW and ITMS methods. This figure shows that despite both ITMS and MSDW detect all blink-events in this segment, ITMS is better at suppressing

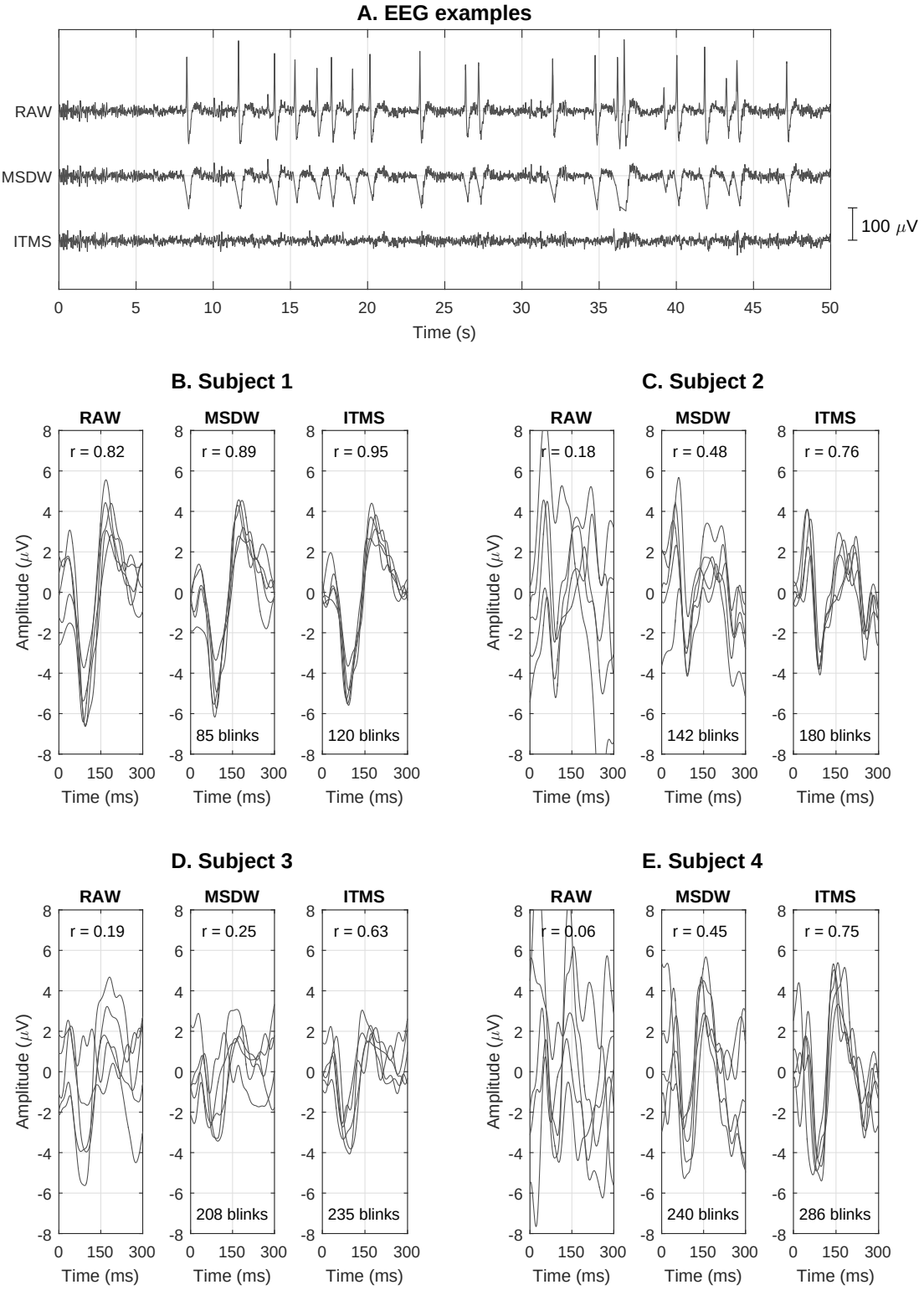

Figure 5. [A] Example of a raw EEG segment (top), and the associated EEGs processed by MSDW (middle) and ITMS (bottom). [B-E] Overlapping CAEP signals obtained in each scenario in 4 subjects. The number of detected blink-events and the mean correlation coefficient (r) between all possible combinations of the CAEP signals from each subject taken two at a time (10 statistics) are shown at the bottom and at the top of the plot respectively.

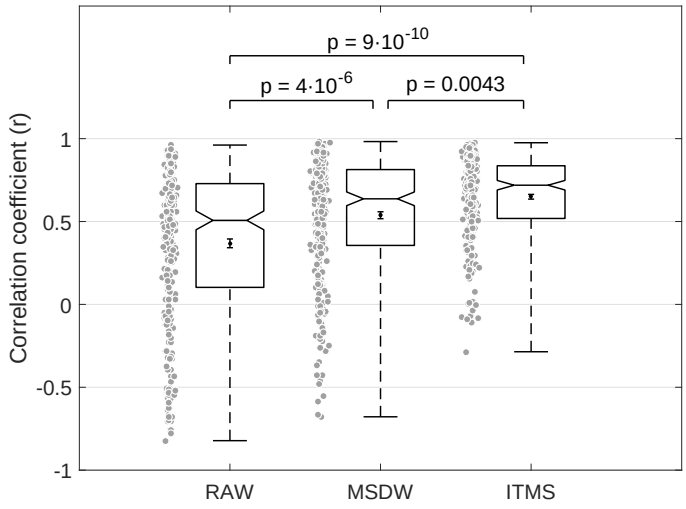

Figure 6. Raw distributions (gray-filled circles), quartile ranges (box plots), and mean and standard error of the mean (errorbars) of the r-distributions obtained for the RAW, MSDW and ITMS secenarios. The p-values at the top of the figure show the levels of significance resulting from the multiple comparison test.

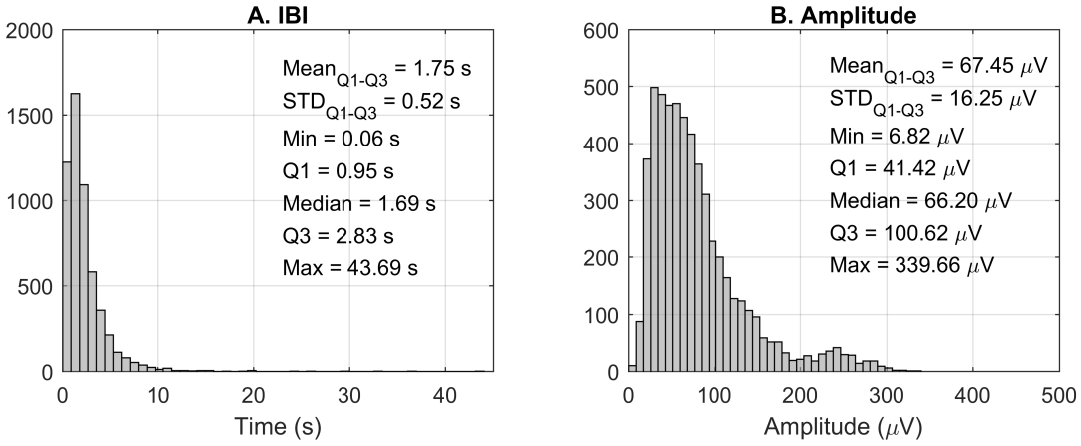

Figure 7. Histograms of the [A] inter-blink interval (IBI, in seconds), and [B] amplitude (in μV) of the blink-events detected in all subjects.

the blink-artifact. Since MSDW assumes that the shape of the artifact is triangular [57], the boundaries of the detected blink-events only include the first positive peak of the artifact. In contrast, ITMS characterizes all components of the blink-artifact waveform, and the suppression is more efficient. Figures 5.B-E show the CAEP signals obtained in each scenario in the first four subjects. The CAEP signals are presented overlapped to allow visual inspection of reproducibility. In each subject and condition, the number at the top of the charts show the mean of the correlation coefficients obtained between all possible combinations of CAEP signals taken two at a time (10 statistics). The individual results obtained in the remaining subjects are shown as supporting material in appendix E.

Figure 6 shows the raw distributions (gray-filled circles), the box plots, and the mean and standard error of the mean (errorbars) for the r-distributions in each analysed scenario. The box plots show the quartile ranges of the distributions (the notch in the boxes indicating the *median*). The *mean* values corresponding to the RAW, MSDW, and ITMS r-distributions are, respectively, 0.37, 0.54, and 0.65. The p-values shown at the top of the figure are the result of the multiple comparison test derived from the Kruskal-Wallis analysis of variance test. The results of this experiment indicate that: (a) both MSDW and ITMS methods improve the quality of CAEP signals; and (b) ITMS presents a statistically significant greater improvement (0.11 greater r-values on average) compared to MSDW.

Figure 7 shows the distributions of the inter-blink interval (IBI) in seconds and the amplitude (in μV) of the blink-events detected in all subjects. This figure shows that on average (estimated as the mean between the first and the third quartile of the distribution), the subjects blinked every 1.75 seconds with an amplitude of 67.45 μV.

4. Discussion

This paper presented in detail and evaluated the performance of the Iterative Template Matching and Suppression (ITMS) technique. This paper showed that (a) ITMS presents an adequate performance in detecting and suppressing blink-artifacts from a single EEG channel; (b) it is fully automatic, since the method does not require any user setup; (c) in contrast to other methods like ICA and DWT (which decompose the EEG signals into a number of components, operate in the transformed domain, and recompose the signals), ITMS is less invasive since the blink-artifact correction only occurs in the contaminated EEG segments; (d) it is robust and stable, as its performance does not strongly depend on the initial blink-artifact template h_0; and (e) the method is easy to implement, since the underlying mathematics are not complex as can be observed in the Matlab script provided as supplementary material.

ITMS aimed to solve two classical limitations of previous methods based on template matching: the selection of the template and the estimate of the threshold. The performance of template matching is highly dependent on the template selection [57]. Previous methods used a library of blink-artifact templates of different waveforms to adapt the inter-subject variability [55, 56], however this approach presented the drawbacks of (a) generating a sufficiently large database of templates, and (b) the selected template would never perfectly match the blink-artifact waveform of the analyzed subjects. In contrast, ITMS solves the problem of template selection through an iterative process. This approach does not require a library of templates, and blink-events detection is performed using a blink-artifact template particular for each analyzed subject.

A second limitation of previously implemented template matching-based methods is that the threshold that separates the blink-events from the noise distribution was selected manually by the user [55, 56], which makes these methods inconsistent

worldwide and dependent on human expertise. Moreover, this paper highlighted the limitations of methods relying on manual thresholds. Firstly, the MSDW threshold suggested by the authors of this technique (threshold equal to 130) did not work well with our data, since the TPR was extremely low in all SNR scenarios (see table 1). And secondly, we observed that (a) a threshold equal to 80 was the most appropriate in our set of real data; (b) this threshold was appropriate with simulated EEGs only in the +5 dB SNR scenario, but it was not efficient when the SNR was high (low TPR) or when the SNR was low (high FPPS); and (c) the most appropriate threshold with the real EEGs from the public database was around 40 in the Fz channel and 60 in the FP1 channel. In contrast, the automatic approach taken by ITMS presented an adequate blink-events detection performance irrespective of the SNR of the test.

This paper also questioned the blink-artifact triangular shape assumption considered by some techniques like MSDW. The blink-artifact waveforms observed across subjects in this study presented a similar morphology, consistent with previous studies [67, 68]: an onset with an abrupt peak following a lower frequency component which extends up to 1 second approximately. Figure 5.A shows an EEG segment contaminated by a number of blink-artifacts (RAW) and the same segment corrected by the MSDW and ITMS methods. This figure shows that the triangular-shape assumption of MSDW allows detection of only the onset peak of the artifact, and therefore, the artifact cannot be completely removed. By contrast, the blink-artifact template estimated by ITMS allows an adequate characterization and suppression of the artifact, which leads to a greater improvement of the quality of the signal of interest (figure 6).

Despite MSDW only allowing blink-artifact detection, we implemented a blink-artifact correction procedure consisting of linear interpolation between the boundaries of the detected blink-artifacts. This approach was followed because, despite other techniques having previously attempted to suppress blink-artifacts in single EEG channel applications, we did not find any alternative satisfactory option. Kanoga and Mitsukura (2014) described a method suppressing from the EEG the frequency components of the blink-events, which are estimated through a 2-step non-negative matrix factorization [67]. However, this method does not allow blink-events detection, and its performance is strongly dependent on the selection of the basis K_1 and K_2, which requires human intervention and with no procedure available to obtain an optimal selection. Rahman and Othman (2015) aimed to solve the need for an EOG reference channel in adaptive filtering by replacing this channel with a softened version of the EEG using a Savitzky-Golay filter [68]. The problem of using a low-pass version of the EEG as a reference is that relevant low frequency EEG components could be suppressed. Majmudar et al. (2015) and Khatun et al. (2016) presented a similar approach based on the discrete wavelet transform (DWT) [69, 70]. This technique basically consists of three steps: decomposing the EEG into a series of high pass and low pass filters, thresholding the coefficients, and recomposing the signal from the filtered components. The major limitation of DWT is that this technique is not efficient when the artifacts overlap in the frequency domain [21].

This paper introduced a number of methodological contributions. First, the weighted average procedure used to estimate the blink-artifact template presents the advantages of (a) counting with a sufficient number of elements on the estimate (an advantage of the mean operator), and (b) avoiding contributions from outliers (an advantage of the median operator). This compromise is particularly relevant when averaging EEG segments, which are often contaminated by large-amplitude transients due to myogenic noise associated with muscular movements of the subjects. Second, the correction applied on the blink-artifact amplitude minimizes the error on the estimates when two or more blink-events are overlapped. Finally, the approach followed in this paper to evaluate blink-events detection is a methodological contribution that overcomes the limitation of the 'true' blink-events ignorance, and that could be useful in future studies to compare the performance of ITMS with other alternative techniques.

Some considerations must be taken into account about ITMS. First, the signal of interest and the blink-artifacts must be uncorrelated, otherwise part of the signal of interest could be modeled as artifact and be suppressed from the EEG. This assumption is not valid if the test requires auditory stimuli presented at very loud levels, i.e. greater than 80 dB HL, since these sounds may evoke an involuntary contraction of the orbicularis oculi muscle (acoustic startle reflex) [65, 66]. Second, ITMS is able to detect, characterize and suppress the artifact associated with the blink activity, but not other types of artifacts like eye saccades, muscular or cardiac activity. Nevertheless, ITMS could be implemented in conjunction with other denoising techniques. Third, the blink-artifact model generated by ITMS represents the LTI component of the blink-artifact, which is unknown. ITMS introduces linear variations in the amplitude of the estimated blink-artifact template to match each blink-artifact detected in the EEG, however it does not account for certain differences in the blink-artifact morphology derived from a violation in the time-invariance assumption; and therefore, it is assumed that ITMS will not completely suppress the blink-artifact process from the EEG. Nevertheless, the results of this study show that eliminating the LTI component of the blink-artifact process improves significantly the quality of CAEP signals (figure 6). Fourth, the benefits of applying the ITMS algorithm would be little if the EEG presents a low number of blink-artifacts or amplitudes significantly lower than the noise floor of the EEG. This is because, on one hand, the ITMS algorithm requires a sufficient number of detected blink-events to provide an accurate estimate of the blink-artifact template; and on the other hand, the detection performance of the ITMS method decreases as the blink-to-EEG ratio decreases (see figure 3). Finally, since ITMS requires the full EEG to operate, this method can only be applied in offline applications.

Acknowledgements

The authors gratefully acknowledge Dr Harvey Dillon (NAL: National Acoustic Laboratories, Sydney, Australia) for his invaluable suggestions at the initial stage of the study; Mrs Ingrid Yeend (NAL) for recruiting and carrying out the audiometry

tests; Mr Mark Seeto (NAL) for his help with the statistical analysis; and Mr Greg Stewart (NAL) for his help with the calibration of the stimuli. The authors would also like to give a special thanks to the editor and to the reviewers for their constructive input to improve earlier versions of this manuscript; as well as to the subjects who participated in the EEG recording sessions of this study. This research was supported by the Australian Government Department of Health and a grant from the National Health and Medical Research Council (grant ID 1063905).

Appendix

Supporting information associated with this article can be found in [URL].

References

[1] Sininger YS (2007). The use of Auditory Brainstem Response in screening for hearing loss and audiometric threshold prediction, in Auditory Evoked Potentials. Basic Principles and Clinical Application, Lippincott Williams & Wilkins, Baltimore, MD, 2007 (Chapter 12).

[2] Krishnaveni V, Jayaraman S, Anitha L, Ramadoss K (2006). Removal of ocular artifacts from EEG using adaptive thresholding of wavelet coefficients. *Journal of Neural Engineering* **3** 338-346.

[3] Lopes da Silva F (2013). EEG and MEG: Relevance to Neuroscience. *Neuron* **80** 1112-1128.

[4] Patel SH, Azzam PN (2005). Characterization of N200 and P300: Selected studies of the Event-Related Potential. *International Journal of Medical Sciences* **2** 147-154.

[5] Wan F, Nan W, Vai MI, Rosa A (2014). Resting alpha activity predicts learning ability in alpha neurofeedback. *Frontiers in Human Neuroscience* **8**, article 500, 7 p.

[6] Klimesch W (1996). Memory processes, brain oscillations and EEG synchronization. *International Journal of Psychophysiology* **24** 61-100.

[7] Hwang G, Jacobs J, Geller A, Danker J, Sekuler R, Kahana MJ (2005). EEG correlates of verbal and nonverbal working memory. *Behavioral and Brain Functions* **1**, 20 p.

[8] Prat CS, Yamasaki BL, Kluender RA, Stocco A (2016). Resting-state qEEG predicts rate of second language learning in adults. *Brain and Language* **157-158** 44-50.

[9] Kuhl PK (2010). Brain mechanisms in early language acquisition. *Neuron* **67** 713-727.

[10] Rothenberger A, Moll GH (1994). Standard EEG and dyslexia in children–new evidence for specific correlates? *Acta Paedopsychiatrica* **56** 209-218.

[11] Boutros NN, Lajiness-O'Neill R, Zillgitt A, Richard AE, Bowyer SM (2015). EEG changes associated with autistic spectrum disorders. *Neuropsychiatric Electrophysiology* **1:3**, 20 p.

[12] Sharma M, Purdy SC, Kelly AS (2014). The contribution of speech-evoked cortical auditory evoked potentials to the diagnosis and measurement of intervention outcomes in children with auditory processing disorder. *Seminars in Hearing* **35** 51-64.

[13] Gratton G (1998). Dealing with artifacts: the EOG contamination of the event-related brain potential. *Behavior Research Methods, Instruments, and Computers* **30** 44-53.

[14] Haggemann D, Naumann E (2001). The effects of ocular artifacts on (lateralized) broadband power in the EEG. *Clinical Neurophysiology* **112** 215-231.

[15] Urigüen JA, Garcia-Zapirain G (2015). EEG artifact removal - State-of-the-art and guidelines. *Journal of Neural Engineering* **12** 031001, 23 p.

[16] Gratton G, Coles MGH, Donchin E (1983). A new method for off-line removal of ocular artifact. *Electroencephalography and Clinical Neurophysiology* **55** 468-484.

[17] Croft RJ, Barry RJ (2000). EOG correction of blinks with saccade coefficients: a test and revision of the aligned-artefact average solution. *Clinical Neurophysiology* **111** 444-451.

[18] Wallstrom GL, Kass RE, Miller A, Cohn JF, Fox NA (2004). Automatic correction of ocular artifacts in the EEG: a comparison of regression-based and component-based methods. *International Journal of Psychophysiology* **53** 105-119.

[19] Croft RJ, Chandler JS, Barry RJ, Cooper NR, Clarke AR (2005). EOG correction: a comparison of four methods. *Psychophysiology* **42** 16-24.

[20] Pham TTH, Croft RJ, Cadusch PJ, Barry RJ (2011). A test of four EOG correction methods using an improved validation technique. *International Journal of Psychophysiology* **79** 203-210.

[21] Sweeney KT, Ward TE, McLoone SF (2012). Artifact removal in physiological signals-practices and possibilities. *IEEE Transactions on Information Technology in Biomedicine* **16** 488-500.

[22] Croft RJ, Barry RJ (2000). Removal of ocular artifacts from the EEG: A review. *Neurophysiologie Clinique/Clinical Neurophysiology* **30** 5-19.

[23] Hesse CW, James CJ (2006). On semi-blind source separation using spatial constraints with applications in EEG analysis. *IEEE Transactions on Biomedical Engineering* **53** 2525-2534.

[24] Mennes M, Wouters H, Vanrumste B, Lagae L, Stiers P (2010). Validation of ICA as a tool to remove eye movement artifacts from EEG/ERP. *Psychophysiology* **47** 1142-1150.

[25] Zhou W, Gotman J (2009). Automatic removal of eye movement artifacts from the EEG using ICA and the dipole model. *Progress in Natural Science* **19** 1165-1170.

[26] Davies ME, James CJ (2007). Source separation using single channel ICA. *Signal Processing* **87** 1819-1832.

[27] Romero S, Mañanas MA, Barbanoj MJ (2008). A comparative study of automatic techniques for ocular artifact reduction in spontaneous EEG signals based on clinical target variables: A simulation case. *Computers in Biology and Medicine* **38** 348-360.

[28] Kierkels JJM, van Boxtel GJM, Vogten LLM (2006). A model-based objective evaluation of eye movement correction in EEG recordings. *IEEE Transactions on Biomedical Engineering* **53** 246-253.

[29] Joyce CA, Gorodnitsky IF, Kutas M (2004). Automatic removal of eye movement and blink artifacts from EEG data using blind component separation. *Psychophysiology* **41** 313-325.

[30] Delorme A, Makeig S (2004). EEGLAB: an open source toolbox for analysis of single-trial EEG dynamics. *Journal of Neuroscience Methods* **134** 9-21.

[31] Jung TP, Humphries C, Lee TW, Makeig S, Mckeown M, Iragui V, Sejnowski TJ (1998). Removing electroencephalographic artifacts: Comparison between ICA and PCA. *Neural Networks for Signal Processing VIII, Proceedings of the 1998 IEEE Signal Processing Society Workshop*, 63-72.

[32] Anderer P, Roberts S, Schlögl A, Gruber G, Klösch G, Hermann W, Rappelsberger P, Filz O, Barbanoj M, Dorffner G, Saletu B (1999). Artifact processing in computerized analysis of sleep EEG - A review. *Neuropsychobiology* **40** 150-157.

[33] Hoffmann S, Falkenstein M (2008). The correction of eye blink artefacts in the EEG: A comparison of two prominent methods. *PLoS ONE* **3**:e3004, 11 p.

[34] Martin BA, Tremblay KL, Stapells DR (2007). Principles and applications of cortical auditory evoked potentials. Basic Principles and Clinical Application, Lippincott Williams & Wilkins, Baltimore, MD, 2007 (Chapter 23).

[35] Van Dun B, Dillon H, Seeto M (2015). Estimating hearing thresholds in hearing-impaired adults through objective detection of cortical auditory evoked potentials. *Journal of the American Academy of Audiology* **26** 370-383.

[36] Ismail N, Sallam Y, Behery R, Al Boghdady A (2017). Cortical auditory evoked potentials in children who stutter. *International Journal of Pediatric Otorhinolaryngology* **97** 93-101.

[37] Barker MD, Kuruvilla-Mathew A, Purdy SC (2017). Cortical auditory-evoked potential and behavioural evidence for differences in auditory processing between good and poor readers. *Journal of the American Academy of Audiology* **28** 534-545.

[38] Ku Y, woo Ahn J, Kwon C, Kim DY, Suh MW, Park MK, Lee JH, Oh SH, Kim HC (2017). The gap-prepulse inhibition deficit of the cortical N1-P2 complex in patients with tinnitus: The

effect of gap duration. *Hearing Research* **348** 120-128.

[39] Bidelman GM, Lowther JE, Tak SH, Alain C (2017). Mild cognitive impairment is characterized by deficient brainstem and cortical representations of speech. *The Journal of Neuroscience* **37** 3610-3620.

[40] Slugocki C, Bosnyak D, Trainor LJ (2017). Simultaneously-evoked auditory potentials (SEAP): A new method for concurrent measurement of cortical and subcortical auditory-evoked activity. *Hearing Research* **345** 30-42.

[41] Duvinage M, Castermans T, Petieau M, Hoellinger T, Cheron G, Dutoit T (2013). Performance of the Emotiv Epoc headset for P300-based applications. *BioMedical Engineering Online* **12**:56, 15 p.

[42] Kawala-Janik A, Baranowski J, Podpora M, Piatek P, Pelc M (2014). Use of a cost-effective neuroheadset EMOTIV Epoc for pattern recognition purposes. *International Journal of Computing* **13** 25-33.

[43] Campbell AT, Choudhury T, Shaohan H, Hong L, Mukerjee MT, Rabbi M, Rajeev DSR (2010). NeuroPhone: Brain-mobile phone interface using a wireless EEG headset. *MobiHeld '10 Proceedings of the second ACM SIGCOMM workshop on Networking, systems, and applications on mobile handhelds* pp. 3-8, New Delhi, India, August 2010.

[44] Nolan H, Whelan R, Reilly RB (2010). FASTER: fully automated statistical thresholding for EEG artifact rejection. *Journal of Neuroscience Methods* **192** 152-162.

[45] Zammouri A, Aitmoussa A, Chevallier S, Monacelli E (2015). Intelligent ocular artifacts removal in a non-invasive single channel EEG recording. *Intelligent Systems and Computer Vision (ISCV)*, 7106164, 5 p, At Fez, Morocco, March 2015.

[46] Aarabi A, Kazemi K, Grebe R, Moghaddam HA, Wallois F (2009). Detection of EEG transients in neonates and older children using a system based on dynamic time-warping template matching and spatial dipole clustering. *NeuroImage* **48** 50-62.

[47] Benedetto S, Pedrotti M, Minin L, Baccino T, Re A, Montanari R (2011). Driver workload and eye blink duration. *Transportation Research Part F: Traffic Psychology and Behaviour* **14** 199-208.

[48] Klein A, Skrandies W (2013). A reliable statistical method to detect eyeblink artefacts from electroencephalogram data only. *Brain Topography* **26** 558-568.

[49] Peng X, Xu J (2016). Hash-based line-by-line template matching for lossless screen image coding. *IEEE Transactions on Image Processing* **25** 5601-5609.

[50] Ahuja K, Tuli P (2013). Object recognition by template matching using correlations and phase angle method. *International Journal of Advanced Research in Computer and Communication Engineering* **2** 1368-1373.

[51] Faundez-Zanuy M (2007). On-line signature recognition based on VQ-DTW. *Pattern Recognition* **40** 981-992

[52] Fu TC, Chung FL, Luk R, Ng CM (2007). Stock time series pattern matching template-based vs. rule-based approaches. *Engineering Applications of Artificial Intelligence* **20** 347-364.

[53] Gong, X, Si YW (2013). Comparison of subsequence pattern matching methods for financial time series. *9th International Conference on Computational Intelligence and Security (CIS), Dec 2013*, 6746375, 154-158.

[54] Skoumal RJ, Brudzinski MR, Currie BS (2015). Distinguishing induced seismicity from natural seismicity in Ohio: Demonstrating the utility of waveform template matching. *Journal of Geophysical Research B: Solid Earth* **120** 6284-6296.

[55] Bizopoulos PA, Al-Ani T, Tsalikakis DG, Tzallas AT, Koutsouris DD, Fotiadis DI (2013). An automatic electroencephalography blinking artifact detection and removal method based on template matching and ensemble empirical mode decomposition. *35th Annual International Conference of the IEEE EMBS, Osaka, Japan, 3-7 July 2013*, 6610883, pp. 5853-5856.

[56] Chang WD, Im CH (2014). Enhanced template matching using dynamic positional warping for identification of specific patterns in electroencephalogram. *Journal of Applied Mathematics*, Article ID 528071, 7 p.

[57] Chang WD, Cha HS, Kim K, Im CH (2016). Detection of eye blink artifacts from single prefrontal channel electroencephalogram. *Computer Methods and Programs in Biomedicine* **124** 19-30.

[58] Turin GL (1960). An introduction to matched filters. *IRE Transactions on Information Theory* **6** 311-329.

[59] Kim S, McNames J (2007). Automatic spike detection based on adaptive template matching for extracellular neural recordings. *Journal of Neuroscience Methods* **165** 165-174.

[60] Huber PJ (2005). Robust statistics, in Wiley Series in Probability and Statistics, New York: John Wiley & Sons, Inc.

[61] Moore BCJ, Creeke S, Glasberg BR, Stone MA, Sek A (2012). A version of the TEN Test for use with ER-3A insert earphones. *Ear and Hearing* **33** 554-557.

[62] Boersma P, Weenink D (2016). Praat: doing phonetics by computer [Computer program]. Version 6.0.17, retrieved 27 April 2016 from www.praat.org.

[63] Elberling C, Don M (2007). Detecting and assessing synchronous neural activity in the temporal domain (SNR, response detection), in Auditory Evoked Potentials. Basic Principles and Clinical Application, Lippincott Williams & Wilkins, Baltimore, MD, (Chapter 5).

[64] Ludbrook J (2008). Statistics in biomedical laboratory and clinical science: Applications, issues and pitfalls. *Medical Principles and Practice* **17** 1-13.

[65] Hahlbrock KH (1962). Auropalpebral-reflex audiometry. *International Journal of Audiology* **1** 261-264.

[66] Ramirez-Moreno DF, Sejnowski, TJ (2012). A computational model for the modulation of the prepulse inhibition of the acoustic startle reflex. *Biological Cybernetics* **106** 169-176.

[67] Kanoga S, Mitsukura Y (2014). Eye-blink artifact reduction using 2-step nonnegative matrix factorization for single-channel electroencephalografic signals. *Journal of Signal Processing* **18** 251-257.

[68] Rahman FA, Othman MF (2015). Eye blinks removal in single-channel EEG using Savitzky-Golay referenced adaptive filtering: a comparison with independent component analysis method. *ARPN Journal of Engineering and Applied Sciences* **10** 18147-18154.

[69] Majmudar CA, Mahajan R, Morshed BI (2015). Real-time hybrid ocular artifact detection and removal for single channel EEG. *IEEE International Conference on Electro/Information Technology (EIT), 21-23 May 2015*, pp. 330-334.

[70] Khatun S, Mahajan R, Morshed BI (2016). Comparative study of wavelet-based unsupervised ocular artifact removal techniques for single-channel EEG data. *IEEE Journal of Translational Engineering in Health and Medicine* **4** 1-8.